An analysis of HF radar measured surface currents to determine tidal, wind-forced, and seasonal circulation in the Gulf of the Farallones, California, United States

Matt K. Gough,[1] Newell Garfield,[1] and Erika McPhee-Shaw[2]

Received 15 July 2009; revised 12 November 2009; accepted 18 November 2009; published 24 April 2010.

[1] A complete year of hourly 3 km resolution high-frequency radar measured surface currents covering the Gulf of the Farallones were analyzed with the following three primary objectives: (1) describe the seasonal surface circulation, (2) identify tidal currents, and (3) determine the influence of wind forcing. Three predominant seasonal circulation regimes were identified: relaxation, storm, and upwelling. The relaxation period exhibited mean poleward flow over the slope, variable equatorward flow over the shelf, and cyclonic and anticyclonic eddies south of Pt. Reyes. The storm period mean flow was variable and exhibited evidence of coastally trapped buoyancy flow from the mouth of the San Francisco Bay. The upwelling period exhibited equatorward flow throughout the gulf with regions of intensified flow at the northern and southern regions over the slope. The tidal variance ranged from 4 to 60%, was highest around the mouth of the Bay, decreased past the shelf, and its spatial pattern reflected the combined influence of the K_1 and M_2 tidal current amplitudes. K_1 ellipses typically rotated clockwise throughout the gulf and decreased in amplitude past the shelf. M_2 ellipses were comparably more variable in orientation and magnitude. Harmonic "tidal" analyses of buoy wind data over 4 month time periods showed significant K_1 amplitudes which did not appear when the analysis was done for the entire year. This indicates that harmonic tidal analyses on surface currents are probably more effective at disassociating diurnal sea breeze driven currents when performed over long periods of time such as a year.

Citation: Gough, M. K., N. Garfield, and E. McPhee-Shaw (2010), An analysis of HF radar measured surface currents to determine tidal, wind-forced, and seasonal circulation in the Gulf of the Farallones, California, United States, *J. Geophys. Res.*, *115*, C04019, doi:10.1029/2009JC005644.

1. Introduction

[2] Three Coastal Ocean Dynamic Radar (CODAR) high-frequency (HF) radar systems have been monitoring the surface currents in the Gulf of the Farallones since May 2006 as part of the California State Coastal Conservancy funded Coastal Ocean Currents Monitoring Program (COCMP). This has provided an unprecedented spatial and temporal view of sea surface currents in this region. Previous studies have examined the complex surface currents in the Gulf of the Farallones using moored acoustic Doppler current profilers (ADCPs) and ship-mounted ADCPs [*Noble et al.*, 1992; *Steger et al.*, 1998, 2000] but these studies did not have the advantage of having a year of continuous hourly 3 km resolution data that is now available with HF radar.

[3] A greater understanding of ocean surface currents in the coastal zone is important for modeling plankton and pollution dispersion, improving hazardous material spill response, and improving search and rescue techniques [*Ullman et al.*, 2003]. This is particularly true in the Gulf of the Farallones where shipping channels and small recreational crafts are subject to powerful and highly variable currents. Recent events in this region involving ineffective oil spill containment and loss of life in recreational boating accidents demonstrate the need for improved drift prediction techniques.

[4] HF radar has been successfully implemented in surface current studies on regions directly to the south at Monterey Bay [*Paduan and Rosenfeld*, 1996] and north at Bodega Bay [*Kaplan et al.*, 2005; *Kaplan and Largier*, 2006], but at this time there have been no studies in the gulf that have used HF radar data for time periods longer than 2 days. Our intent is to not only bridge the gap between *Paduan and Rosenfeld* [1996] and *Kaplan et al.* [2005], but to gain a better understanding of the uniquely strong tidal influence on the currents in the gulf due to its proximity to the mouth of the San Francisco Bay.

[1] Romberg Tiburon Center for Environmental Studies, San Francisco State University, Tiburon, California, USA.
[2] Moss Landing Marine Laboratories, San Jose State University, Moss Landing, California, USA.

0148-0227/10/2009JC005644

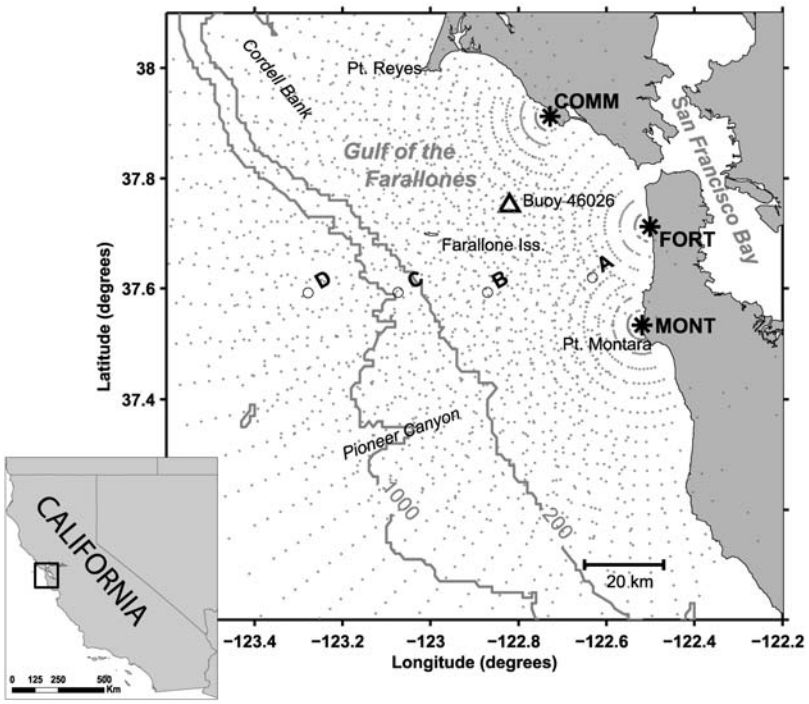

Figure 1. Gulf of the Farallones study area. The box in the index map of California outlines the study area. Grey lines denote the 200 and 1000 m bathymetry contours. CODAR stations are denoted with stars (COMM, Commonweal; FORT, Fort Funston; MONT, Montara). Small gray points are radial data points for each station. Four cross-shore coordinate points used in detailed harmonic tidal analyses are labeled A (37.620°N, 122.632°W), B (37.593°N, 122.870°W), C (37.593°N, 123.074°W), and D (37.592°N, 123.278°W).

[5] The Gulf of the Farallones encompasses the region on the continental shelf bounded by the 200 m isobath to the west, the California coastline to the east, Pt. Reyes (38.0°N) to the north, and Pt. Montara (37.5°N) to the south. The area of this study extends beyond the Gulf of the Farallones to the west and to the south (Figure 1). Both the coastline and the bathymetry in this region are complex. The coastline has two significant points, Pt. Reyes and Pt. Montara, where Pt. Reyes, the larger of the two, extends seaward about 20 km. The mouth of the San Francisco Bay is at the eastern edge of the Gulf of the Farallones. The continental shelf widens here to approximately 50 km offshore and multiple canyons extend outward from the coast and across the shelf and slope. The Farallon Islands are a string of small islands about 40 km offshore near the western edge of the shelf.

[6] There have been numerous publications on oceanic circulation along the northern California coast that were derived from several collaborative programs. Among these programs were the Coastal Ocean Dynamics Experiment (CODE) during the spring-summer months of 1981 and 1982 [*Beardsley and Lentz*, 1987], Coastal Transition Zone Program (CTZ) [*Brink and Cowles*, 1991], Northern California Coastal Circulation Study (NCCCS) sponsored by the Minerals Management Service of the U.S. Department of the Interior from March 1987 to October 1989, and Wind Events and Shelf Transport (WEST) [*Largier et al.*, 2006]. The primary goals of these studies were to gain a better understanding of coastal wind-driven upwelling patterns and their effects on biological productivity. Although most of these studies were focused on the regions to the north, their findings on general circulation trends are applicable to the Gulf of the Farallones.

[7] Equatorward flow along the northern California coast is driven by persistent winds from the northwest during the spring and summer months. With wind relaxation, which typically occurs during the fall and winter months, poleward flow is driven by a poleward pressure gradient [*Gan and Allen*, 2002; *Hickey and Pola*, 1983; *Largier et al.*, 1993; *Lynn and Simpson*, 1987; *Steger et al.*, 2000]. Discrepancies between studies regarding the timing of these seasonal flow patterns are most likely due to natural seasonal variability.

[8] From the NCCCS, three seasonal regimes were identified that characterize the flow patterns along the northern California coast [*Largier et al.*, 1993]: (1) upwelling (April–July), caused by persistent winds from the northwest associated with a synoptic-scale atmospheric surface high pressure over the northeast Pacific Ocean and surface low over the southwest United States; (2) relaxation (August–November), due to a release of upwelling-favorable winds which allow a poleward barotropic pressure gradient to come into effect; and (3) storm (December–March), where surface currents are driven by storm-related wind events.

[9] In the Gulf of the Farallones, *Steger et al.* [2000] found August to have poleward flow over the shelf and at the coast and equatorward flow in the northern region 20–50 km off the coast. This equatorward flow was observed to surface at approximately 60 km from the shelf break. In February, strong poleward flow (Slope Countercurrent)

was observed over the continental slope along with equatorward flow over the continental shelf. A subsurface jet from the north came around Pt. Reyes and decelerated in the gulf. There was generalized offshore flow at the surface and toward shore flow below the surface which was attributed to Ekman processes. In May, a convergence of poleward and equatorward jets was observed at the continental slope and where the two jets converged there was strong westward flow.

[10] High-frequency currents (tidal, inertial, and diurnal wind driven) have received less attention. Shelf and slope tidal currents in the region north of the gulf were examined by *Noble et al.* [1987] and *Kaplan et al.* [2005]. In this region the M_2 tidal constituent has the highest amplitudes of all constituents and usually contains 50–75% of the tidal variance [*Noble et al.*, 1987]. Over the middle slope the M_2 barotropic variance drops below 50%, suggesting influence of the M_2 baroclinic tide [*Noble et al.*, 1987]. Spatial and temporal variability in the M_2 tidal ellipses were suggested to be caused by perturbations in the M_2 barotropic tide acting as a coastally trapped Kelvin-like wave affected by variations in the coastal boundary as it propagated poleward. Diurnal phases of current ellipses such as the barotropic K_1 were uniform over the deeper basin but changed dramatically over the slope. Diurnal ellipses over the basin and the upper slope were narrow and rotated counterclockwise. However, over the middle slope, between these two regions, they were found to rotate clockwise with variable phase shifts. These diurnal barotropic currents were thought to propagate poleward as a combination of Kelvin and continental shelf waves trapped along the coast.

[11] In this study we analyze a year of HF radar data to describe the seasonal surface circulation in the Gulf of the Farallones. In order to do this, we examine mean monthly surface circulation patterns, the influence of the particularly strong tidal currents in the region, and the influence of wind stress.

2. Data and Methods

[12] This study is primarily based on a year of hourly 3 km resolution HF radar surface current data in the Gulf of the Farallones starting 1 September 2006 and ending 31 August 2007. These data are used along with hourly wind data from NDBC buoy 46026.

2.1. HF Radar Data

[13] Surface currents can be determined by measuring backscattered HF radar signals emitted from shore-based antennas [*Barrick and Lipa*, 1979]. At least two (and preferably more) HF radar stations with overlapping ranges are necessary to compute the two-dimensional surface flow from the radial data. Geometric dilution of precision (GDOP) error is largest along antenna pair baseline and in the far field where the look angles are similar [*Chapman et al.*, 1997].

[14] The credibility of HF radar data has been tested in a number of studies by making comparisons with moored ADCPs, ship-mounted ADCPs, drifters and models [*Carbajal and Pohlmann*, 2004; *Chapman et al.*, 1997; *Kaplan et al.*, 2005; *Kohut and Glenn*, 2003; *Ohlmann et al.*, 2007; *Paduan and Rosenfeld*, 1996; *Paduan et al.*, 2006; *Wright*, 2008]. These studies have shown that comparisons between HF radar velocities with other types of measurements produce RMS differences between 3 and 20 cm/s. The estimated precision of the HF radar radial velocities is believed to be about 4 cm/s [*Paduan and Rosenfeld*, 1996]. *Chapman et al.* [1997] points out that even with HF radar errors as large as 8 cm/s, the standard deviation within a single frequency bin (such as a tidal frequency) for at 1100 point time series would be approximately 0.34 cm/s. It should also be noted that, since HF radar noise is random, standard errors decrease as the length of the time series increases in mean calculations.

[15] There have been two studies that have investigated HF radar errors in the gulf. The first study was during NOAA's 2006 Safe Seas Oil Spill Response Drill [*Long*, 2007]. In this 2 day (48 hour) exercise, strong correlations between Quick Release Environmental Buoys (QREB) equipped with ADCPs and HF radar total vectors were found in both the long-shore and cross-shore components with R^2 values of 0.90 and 0.69, respectively [*Long*, 2007]. The second study, which analyzed HF radar radial uncertainties in January and April 2008, found RMS differences between HF radar measurements and in situ drifting buoys to range from 9.0 to 19.1 cm/s [*Wright*, 2008].

[16] San Francisco State University/Romberg Tiburon Center, as part of the statewide COCMP, operates the three HF radar stations used in this study to measure surface currents in the Gulf of the Farallones. The stations are named COMM (Commonweal), FORT (Fort Funston), and MONT (Montara; Figure 1). Each of the three 12–13 MHz systems has an effective range of approximately 75 km.

[17] We used CODAR Ocean Systems software to process and combine hourly radial data from the three stations and to create hourly total vector data. Only calibrated (measured) antenna patterns were used to process radial data [*Lipa et al.*, 2006]. Data points were discarded beyond a GDOP distant angular limit of 30° and within a baseline angular limit of 20°. In order to improve the accuracy, the radial data are averaged over set time periods (readings every 10 min are averaged over 1 hour for this study). A least squares fit of radial vectors within a specified radius (6 km in this case) are used to calculate 2-D flow on a 3 km grid. These 2-D flow data are referred to as total vectors and contain hourly U (east–west) and V (north–south) velocity components at each grid point. Only total vector data points with at least 70% temporal coverage were kept (Figure 2), which reduced the number of total vector data points by 41%. The remaining 442 total vector data points used in this study cover an area of approximately 4000 km^2.

2.2. Harmonic Tidal Analyses on HF Radar Data

[18] We used T_tide, an open source MATLAB toolbox as described by *Pawlowicz et al.* [2002], to separate out the tidal from the nontidal components of the currents by performing a harmonic tidal analysis on HF radar measured currents. There are limitations using harmonic tidal analyses such as T_tide. It is difficult to separate the K_1 lunisolar frequency (1.003 cycles per day (cpd)) from the P_1 principal solar diurnal frequency (0.997 cpd) and separate the S_2 principal solar frequency (2 cpd) from the first harmonic of the true diurnal signal [*Kaplan et al.*, 2005]. Winds, particularly in the spring and summer months, have diurnal

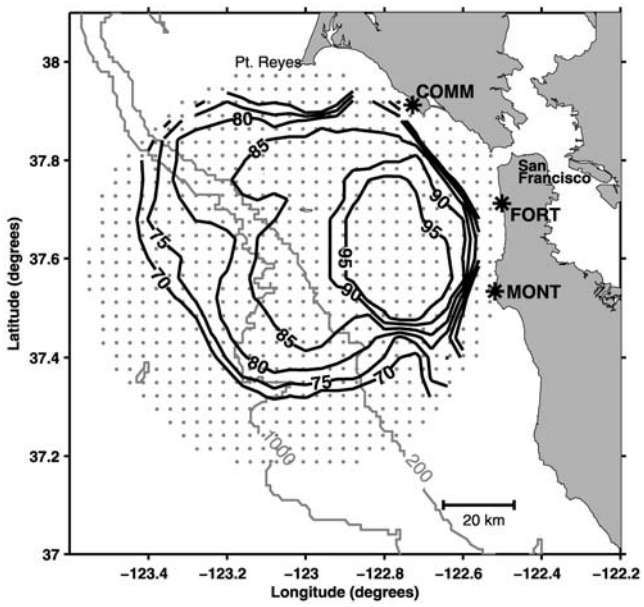

Figure 2. Percent contours of HF radar temporal data coverage for the year September–August 2006–2007. Grey dots indicate total vector data points on 3 km grid. Only data points with at least 70% coverage were used in this study. Contours below 70% are not shown.

frequencies similar to the K_1 and P_1 tidal forcings and are believed to contribute to the tidal energy at those frequencies [*Kaplan et al.*, 2005]. Also, harmonic analysis only identifies phase-locked barotropic tides and not internal baroclinic tides which are not phase locked. This is important since there is evidence that internal tides often dominate the cross-slope current component along the northern California middle slope [*Noble et al.*, 1987].

[19] Two sets of harmonic tidal analyses were performed on all total vector data points for the year of HF radar data. In the first set, harmonic tidal analyses were performed on three 4 month time series of hourly complex-valued currents (September–December 2006, January–April 2007, and May–August 2007). In the second set, harmonic tidal analyses were performed on a continuous year of hourly complex-valued current data (September 2006 to August 2007).

[20] Detailed T_tide harmonic tidal analyses were performed at four across-shelf locations (A–D in Figure 1; see Table 1) using a year of hourly complex-valued HF radar current data. The locations were chosen for maximum data coverage as well as their proximity to NDBC buoy 46026 to allow comparisons with the wind data. Point A is the most inshore point where we expect to see the strong influence of flow though the Golden Gate, point B is midshelf and within 20 km of buoy 46026, point C is on the outer shelf and D is over the slope. Only constituents with significant amplitudes and signal-to-noise ratios are listed in the harmonic tidal analysis tables (Tables 1–3).

[21] Residual currents were calculated by subtracting the tidal prediction time series from the original HF radar measured time series. Time series plots of original HF radar measured surface currents, tidal currents, residual currents and pl64 low-pass filtered currents [*Beardsley et al.*, 1985] in the V direction (north–south) at location B for a year of data are shown in Figure 3. The U direction (east–west) time series plots are not shown because their amplitudes were significantly smaller than those in the V direction and their tidal signal less pronounced.

Table 1. Summary of Harmonic Tidal Analysis Ellipse Characteristics for the Year September 2006 to August 2007 at Points A, B, C, and D[a]

Constituent	Major Axis (cm/s)	Minor Axis (cm/s)	Inclination (deg)	Phase (deg)	Signal-to-Noise Ratio
		Point A[b]			
O_1	4.5	−1.5	92.9	84.9	14
P_1	2.8	−1.1	74.9	86.8	5.5
K_1	9.4	−2.2	85.0	98.3	74
N_2	2.4	0.03	78.8	110.7	17
M_2	11.3	0.3	83.5	132.8	280
S_2	3.3	0.9	100.1	170.8	36
K_2	1.1	0.3	104.6	162.5	4.3
		Point B[c]			
O_1	4.4	−2.1	99.0	91.8	13
P_1	1.5	−0.6	50.2	107.5	2.1
K_1	7.8	−3.0	87.2	114.8	35
N_2	0.9	0.2	86.8	115.1	4.1
M_2	5.0	1.6	81.3	137.2	98
S_2	1.7	0.6	124.9	191.8	16
K_2	0.8	0.3	106.3	165.9	3.4
		Point C[d]			
O_1	3.5	−1.6	86.5	121.1	11
P_1	1.3	−1.0	154.5	9.5	3.1
K_1	5.6	−1.8	73.5	150.5	25
N_2	0.8	0.2	40.0	56.0	3.3
M_2	3.5	1.0	88.2	147.3	35
S_2	1.6	0.6	132.7	230.6	11
K_2	1.0	0.2	84.5	131.5	2.7
		Point D[e]			
SSA	4.3	0.5	167.1	254.3	1.5
O_1	2.0	−0.3	90.6	159.4	2.8
P_1	2.0	−1.1	116.9	56.2	3.5
K_1	2.6	−0.3	69.6	141.9	6.7
N_2	0.7	−0.02	29.2	127.8	1.3
M_2	2.9	−1.2	96.5	124.3	2.5
S_2	1.1	−0.3	42.1	88.2	2.5
K_2	1.1	0.1	31.0	89.5	2.8

[a]Only constituents with significant amplitudes and signal-to-noise ratios are listed.
[b]Percent total variance is 32.8%.
[c]Percent total variance is 14.9%.
[d]Percent total variance is 8.9%.
[e]Percent total variance is 5.2%.

2.3. Wind Data

[22] Within the Gulf of the Farallones at 37.75°N, 122.82° W, NDBC buoy 46026 reports hourly wind speed and wind direction from an anemometer 5m above sea level. Hourly wind stress data used in spectral analyses were calculated from hourly buoy 46026 wind data (converted to 10 m above sea level) using the Air-Sea Matlab toolbox function

Table 2. Summary of Harmonic Tidal Analysis on Buoy 46026 Winds for the Year September 2006 to August 2007[a]

Constituent	Major Axis (m/s)	Minor Axis (m/s)	Inclination (deg)	Phase (deg)	Signal-to-Noise Ratio
K1	0.2	0.1	30.1	43.2	1.3
S2	0.3	−0.1	126.8	202.2	7.6
K2	0.1	−0.02	119.0	141.3	2

[a]Percent total variance is 0.5%.

Table 3. Summary of Harmonic Tidal Analysis on Buoy 46026 Winds for the Time Periods September–December 2006, January–April 2007, and May–August 2007

Constituent	Major Axis (m/s)	Minor Axis (m/s)	Inclination (deg)	Phase (deg)	Signal-to-Noise Ratio
		September–December 2006			
O_1	0.3	−0.1	159.2	39.8	1.2
K_1	1.1	−0.1	156.2	169.4	9.9
J_1	0.5	0.1	130.7	255.8	2.4
M_2	0.1	−0.001	169.8	265.6	1
S_2	0.3	−0.2	122.8	222.8	6
		January–April 2007			
NO_1	0.3	−0.01	116.1	81.6	1.4
K_1	1.0	−0.5	157.4	288.3	15
J_1	0.3	−0.1	113.0	150.1	1.2
L_2	0.2	0.01	111.6	202.7	1.2
S_2	0.4	−0.8	137.9	179.6	5.9
		May–Auust 2007			
K_1	0.9	−0.3	131.9	75.2	13
J_1	0.2	0.01	139.4	327.4	1.1
S_2	0.2	−0.1	100.9	219.0	2.2

stresslp.m which implements $\vec{\tau} = \rho C_D |w| \vec{w}$ to calculate neutral wind stress following *Large and Pond* [1981].

2.4. Harmonic "Tidal" Analysis on Buoy 46026 Winds

[23] Like the harmonic tidal analysis on HF radar current data, there were two parts to the harmonic tidal analysis on buoy 46026 wind data. The first analysis on hourly complex-valued wind data was performed over a continuous year and the second analysis was performed over three 4 month time periods.

2.5. Rotary Spectral Analyses on HF Radar Measured Surface Currents and Buoy 46026 Winds

[24] Rotary spectral analyses [*Gonella*, 1972], implementing an oceanographic adaptation of Matlab's PSD function (F. Bahr, personal communication, 2007), were performed on 1 year of HF radar surface current data at location B and on 1 year of wind stress data from buoy 46026 (Figure 4). All data gaps were linearly interpolated. Rotary spectral analyses were also performed on 11 separate time periods between 603 and 865 hours (approximately 1 month) during the year in which data gaps larger than 12 hours in the HF radar data were avoided. Of these 11 spectral analyses, two are pictured to demonstrate seasonal variability (Figures 5 and 6).

3. Seasonal and Mean Monthly Surface Flow Patterns

[25] Observed surface flow patterns can be placed into the following three categories based upon generalized relaxation/storm/upwelling seasonal trends: (1) relaxation, October–December 2006, characterized by mean poleward flow over the slope coinciding with light and variable winds; (2) storm, January–February 2007, when there was no longer a well-defined mean poleward flow over the slope and currents were influenced by highly variable storm-driven winds; and (3) upwelling, March–August 2007, characterized by mean equatorward flow and upwelling-favorable winds throughout the region, along with persistent divergence patterns. Since the flow patterns are largely dependent on the winds, which can have considerable interannual variability, the time frames of these categories do not completely agree with previous studies [*Huyer et al.*, 1998; *Largier et al.*, 1993; *Lynn and Simpson*, 1987; *Noble and Ramp*, 2000; *Steger et al.*, 2000].

[26] On multiple occasions during the year, hourly current velocities reached 50–60 cm/s. These strong wind-driven surface current events were equatorward during the upwelling season and equatorward and poleward during the storm season.

[27] In this section we describe surface flow patterns for each month since many features in the flow patterns cannot be seasonally categorized. The mean monthly surface flow field of September 2006 appears to represent a transition period at the end of the upwelling season (Figure 7a). The mean monthly winds at buoy 46026 were fairly strong at 3.7 m/s out of the Northwest. There was light equatorward flow over the shelf and a gradual change in direction at the slope to a more westward direction (Figure 7a). The mean westward flow over the slope is probably due to periodic poleward flow in this region averaged into the calculations. There is a hint of poleward flow following the coastline between the mouth of the Bay and Pt. Reyes.

[28] October 2006 marked the beginning of the relaxation period as mean winds were light and variable (Figure 7b). There was the usual equatorward flow over the shelf but at the midshelf and slope there was significant poleward flow with mean velocities reaching 15 cm/s. Variations of this poleward flow over the slope remained until February.

[29] In November the mean winds increased to 3.0 m/s out of the Northwest. Equatorward flow over the shelf intensified from October in response to the winds and the poleward flow over the slope weakened (Figure 7c). The dominant zone of cross-shelf shear, where mean poleward flow over the shelf met mean equatorward flow over the slope, followed the 200 m isobath through almost the entire gulf.

[30] The mean wind speed for December was very light at 0.6 cm/s (Figure 7d) which was due to frequent reversals in direction associated with storms (Figure 3). The mean flow was almost completely poleward except for an area south of Pt. Reyes. Like October, the mean poleward flow over the slope reached 15 cm/s. There was strong mean poleward flow following the coastline between the mouth of the Bay and Pt. Reyes.

[31] In January 2007 the mean surface current flow was completely reversed from December and was predominantly equatorward throughout the gulf reflecting the mean winds at the SF buoy which increased from December to 3.7 m/s out of the north–northwest (Figure 7e). There was no mean poleward relaxation flow over the slope and there was a region of strong southwestward flow at the eastern boundary of the gulf.

[32] The mean winds in February decreased from January to 2.1 m/s and were from the west–northwest. Mean flow was complex and probably affected by storm-driven winds. There was strong poleward flow over the inner shelf between the mouth of the Bay and Pt. Reyes, equatorward flow over the outer shelf, and westward flow over the slope (Figure 7f). An eddy pattern in the mean monthly surface flow at 37.7 N, 122.8 W developed between the inner shelf poleward flow and outer shelf equatorward flow.

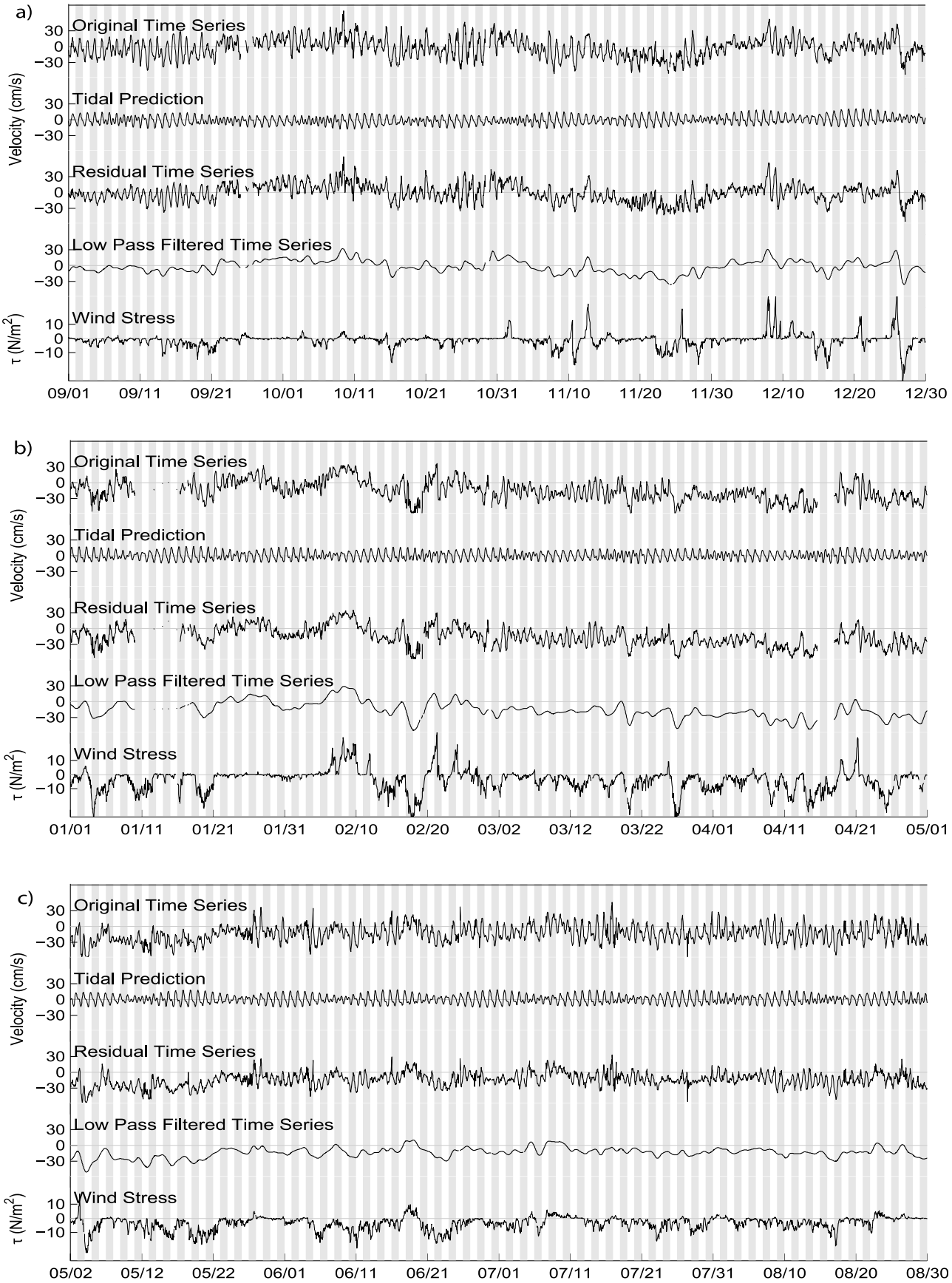
a)
Original Time Series
Tidal Prediction
Residual Time Series
Low Pass Filtered Time Series
Wind Stress
Velocity (cm/s)
τ (N/m²)
30
0
−30
10
−10
09/01 09/11 09/21 10/01 10/11 10/21 10/31 11/10 11/20 11/30 12/10 12/20 12/30
b)
Original Time Series
Tidal Prediction
Residual Time Series
Low Pass Filtered Time Series
Wind Stress
Velocity (cm/s)
τ (N/m²)
01/01 01/11 01/21 01/31 02/10 02/20 03/02 03/12 03/22 04/01 04/11 04/21 05/01
c)
Original Time Series
Tidal Prediction
Residual Time Series
Low Pass Filtered Time Series
Wind Stress
Velocity (cm/s)
τ (N/m²)
05/02 05/12 05/22 06/01 06/11 06/21 07/01 07/11 07/21 07/31 08/10 08/20 08/30

Figure 3

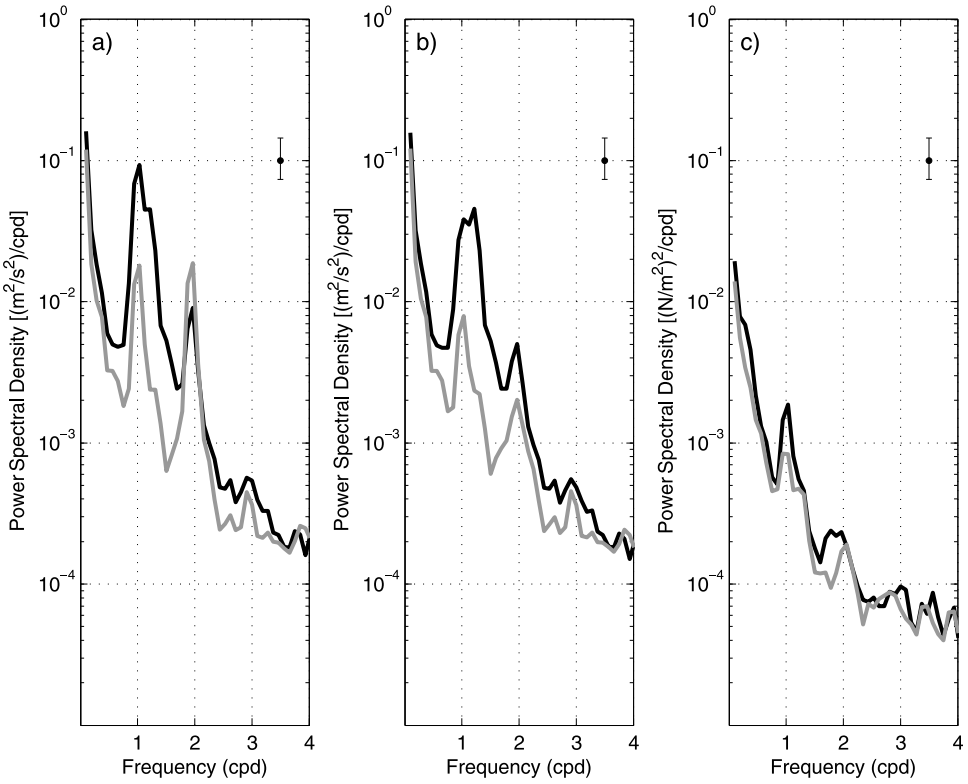

Figure 4. Power spectral densities of (a) HF radar current velocities, (b) residuals at location B, and (c) wind stress from buoy 46026 wind data for the year 1 September 2006 to 31 August 2007. The black line indicates clockwise rotation and the gray line indicates counterclockwise rotation. The 95% confidence interval is shown in the upper right corner. Frequency is in cycles per day (cpd).

[33] With March came the onset of the upwelling season as mean monthly winds out of the northwest markedly increased to 5.2 m/s and drove the surface flow equatorward throughout the region (Figure 8a). Two large areas over the slope (one to the north and one to the south) had mean monthly current velocities from the northwest of over 30 cm/s. These two areas also experienced significant divergence in the flow and were separated by a region of convergence [*Gough*, 2008]. To varying degrees, this pattern in the surface flow and divergence is evident through the entire upwelling season to August 2007. The intense flow southwest of Pt. Reyes is likely a wind-driven phenomenon as southward surface wind accelerations have been observed off coastal points such as Pt. Arena and Pt. Sur along the California coast [*Dorman et al.*, 2000]. The region directly south of Pt. Reyes appears to be partially sheltered from the northwesterly winds and this was where surface flows were weakest (note that this area had small tidal variance (Figure 9). Weak mean flow over the inner shelf is due, in part, to the tidal influence where flow is continuously reversing direction.

[34] April was similar to March. Mean wind speeds increased to 6.2 cm/s and mean surface flow was equatorward throughout the gulf (Figure 8b). The two regions of divergence found in March were strongly enhanced [*Gough*, 2008]. Of all the months, April exhibited the strongest mean winds, the strongest divergence, and the strongest mean surface currents. As in March, mean surface currents reached over 30 cm/s in some areas. This pattern continued into May (Figure 8c).

[35] June had the second highest mean wind speeds (5.7 m/s; Figure 8d) yet the maximum mean surface current flows were noticeably weaker than those found in March and May. In July and August the mean winds decreased to 4.1 and 3.8 cm/s, respectively (Figures 8e and 8f). The decrease in mean winds reflected a decrease in surface flow and divergence although the general upwelling season surface current pattern remained the same.

4. Tidal Currents

[36] The total tidal variance varied between 4% and 60% in the gulf. In general, the highest tidal variances were found

Figure 3. Current velocity hourly time series at location B in the V direction (north–south) for original HF radar time series, the tidal prediction, residuals, pl64 low-pass filtered time series, and wind stress for (a) September–December 2006, (b) January–April 2007, and (c) May–August 2007. Here 24 hour periods are indicated by alternating white and gray vertical bars. Tidal prediction was generated by a harmonic tidal analysis. Residual currents are the tidal prediction subtracted from the original time series. Current velocities are in cm/s and wind stress (τ) is in N/m^2.

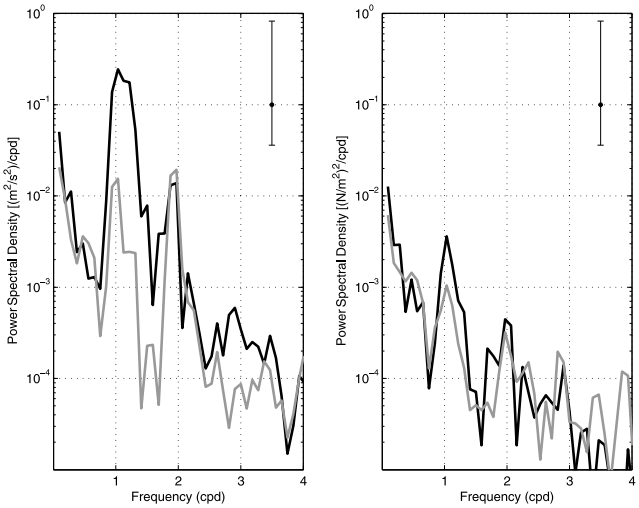

Figure 5. Power spectral densities of (left) HF radar velocities at location B and (right) wind stress from buoy 46026 wind data for the time period 1–26 September 2006. The black line indicates clockwise rotation and the gray line indicates counterclockwise rotation. The 95% confidence interval is shown in the upper right corner. Frequency is in cpd.

along the region nearest to the mouth of the Bay and the lowest tidal variances were found beyond the continental slope (Figure 9). The K_1 and M_2 tidal constituents dominated the tidal currents and the spatial pattern of their respective amplitudes (Figure 10) reflects the spatial pattern in the tidal variance (Figure 9).

4.1. Harmonic Tidal Analyses on Surface Currents

[37] The total tidal variance for the entire year at locations A–D (from nearshore to farshore) was 32.8%, 14.9%, 8.9%, and 5.2%, respectively (Table 1). The variance was typically much larger in the V direction (north–south) compared to the U direction (east–west) [*Gough*, 2008]. The K_1 and M_2 ellipse major axis amplitudes were the largest of all other constituents at locations A–D and decreased from nearshore to farshore like the tidal variance (K_1: 9.4, 7.8, 5.6, and 2.5 cm/s, M_2: 11.3, 5.0, 3.5, and 2.9 cm/s) (Table 1). The spatial pattern of the total tidal variance was bulls eyed around the mouth of the San Francisco Bay which demonstrates the extent of the strong tidal flow in and out of the mouth (Figure 9). There is some indication that tidal variance was depth dependent since percentage contours are bulls eyed around the Farallon Islands and decrease beyond the 200 m bathymetric contour.

[38] In general, the spatial pattern of the M_2 major axis amplitudes exhibited more spatial variability than the K_1 pattern which agrees with previous studies to the north [*Kaplan et al.*, 2005; *Noble et al.*, 1987]. The K_1 major axis amplitudes seem to be somewhat correlated with depth as there were generally higher amplitudes over the shelf and around the Farallon Islands (similar to the total tidal variance pattern in Figure 9) (Figure 10a). An exception to this occurs south of Pt. Reyes where K_1 amplitudes decrease. K_1 amplitudes over the shelf ranged between 5 and 12 cm/s and decreased to about 3 cm/s past the 200 m isobath. The M_2 had two areas where the amplitudes were notably small (less than 3 cm/s). One of these areas was just south of Pt. Reyes and the other was centered at 37.55°N, 123.1°W.

[39] The K_1 ellipses were roughly oriented along shore over the shelf whereas the M_2 ellipses were oriented along shore only over the southern region of the shelf (Figure 11). The highest amplitudes were observed near the mouth of the Bay where ellipses show a strong clockwise (CW) rotational influence and decreased eccentricity for both the K_1 and M_2 constituents. The M_2 tidal ellipse patterns were more variable in magnitude and direction and there is an indication that the rotational direction of M_2 ellipses switch from counterclockwise (CCW) over the shelf to CW over the slope.

[40] Although the K_1 and M_2 frequencies typically had the largest influence on the tidal currents over the slope, the O_1 had ellipse major axis amplitudes of 3.5 and 2.0 cm/s at locations C and D which were comparable to the K_1 and M_2 amplitudes (Table 1).

[41] Tidal analyses on separate 4 month time periods showed significant variability. These differences illuminate the importance of choosing longer time periods such as a year. The K_1 major axis amplitudes along the inner shelf went from 10–12 cm/s (September–December), to 2–8 cm/s (January–April), to 8–14 cm/s (May–August) (Figure 12). The spatial structure of the K_1 major axis amplitudes also varied widely between the three time periods (Figure 12) although the M_2 amplitudes did not vary nearly as much [*Gough*, 2008]. These results are reflected in the total tidal variance where the variance reached 50–60% along the inner shelf during the first and third time periods and only 28% in the second time period [*Gough*, 2008]. Harmonic analyses on monthly time periods, although not reported in this paper, further confirm these findings.

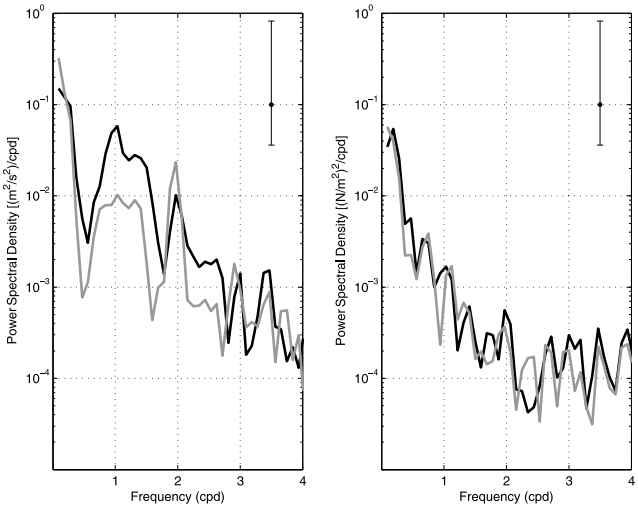

Figure 6. Power spectral densities of (left) HF radar velocities at location B and (right) wind stress from buoy 46026 wind data for the time period 15 February to 17 March 2007. The black line indicates clockwise rotation and the gray line indicates counterclockwise rotation. The 95% confidence interval is shown in the upper right corner. Frequency is in cpd.

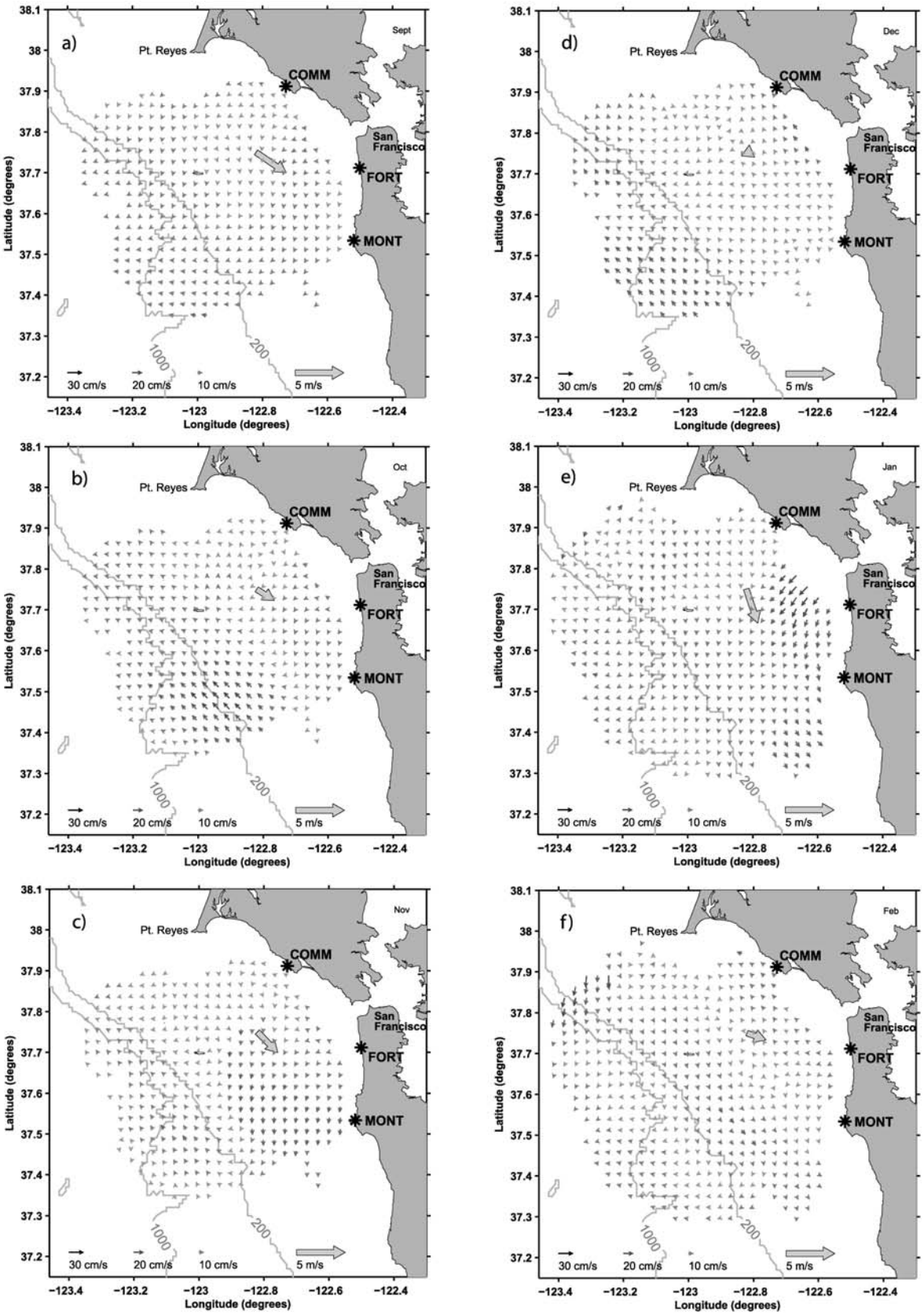

Figure 7. Mean monthly surface flow for (a) September, (b) October, (c) November, (d) December, (e) January, and (f) February. Magnitude is indicated by both the length and gray scale of the arrows. Black arrows indicate means greater than 25 cm/s. The large gray arrow indicates direction and magnitude of mean winds at buoy 46026 in m/s. Arrows are provided at the bottom for scaling.

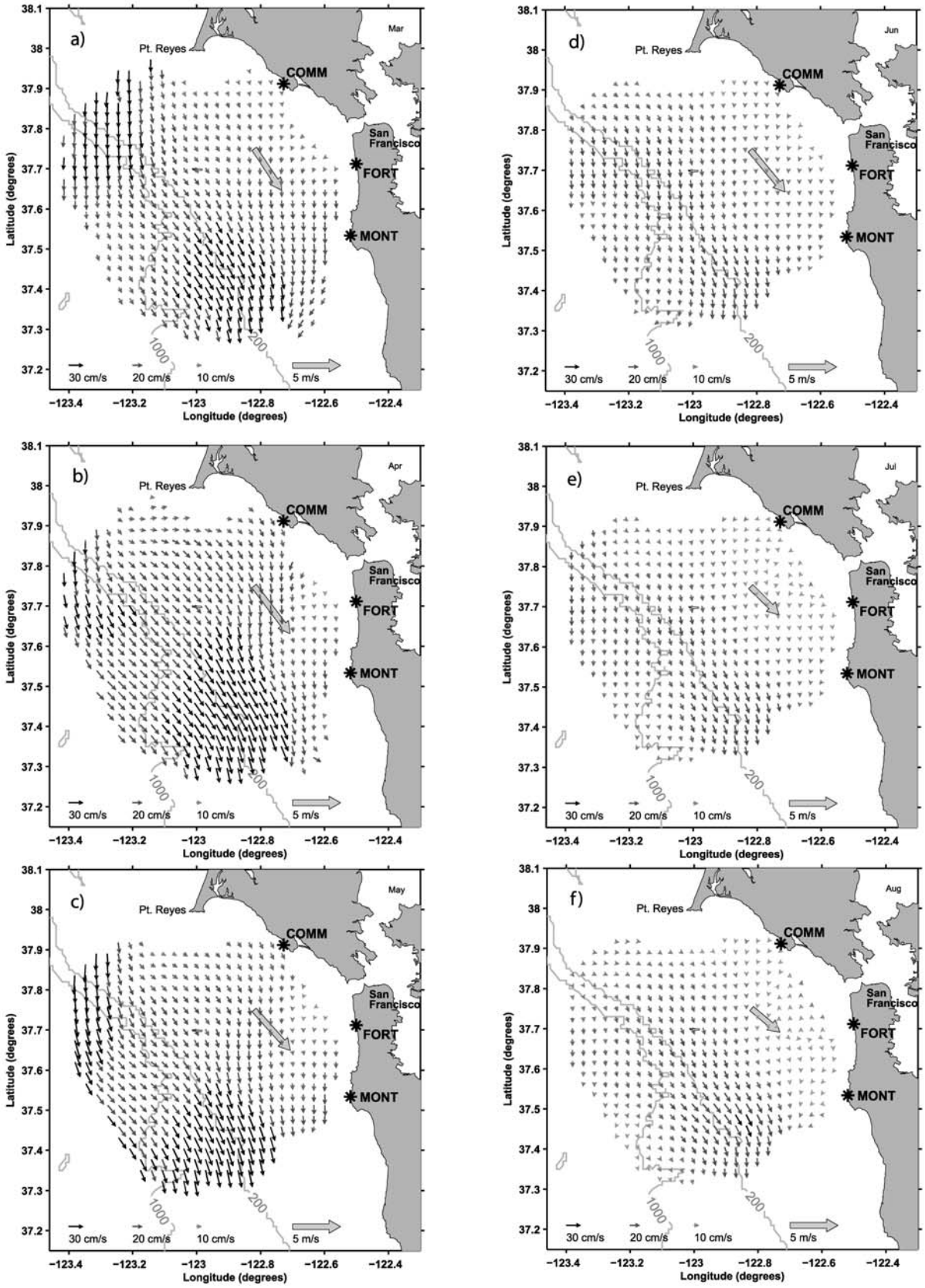

Figure 8. Mean monthly surface flow for (a) March, (b) April, (c) May, (d) June, (e) July, and (f) August. Magnitude is indicated by both the length and gray scale of the arrows. Black arrows indicate means greater than 25 cm/s. The large gray arrow indicates direction and magnitude of mean winds at buoy 46026 in m/s. Arrows are provided at the bottom for scaling.

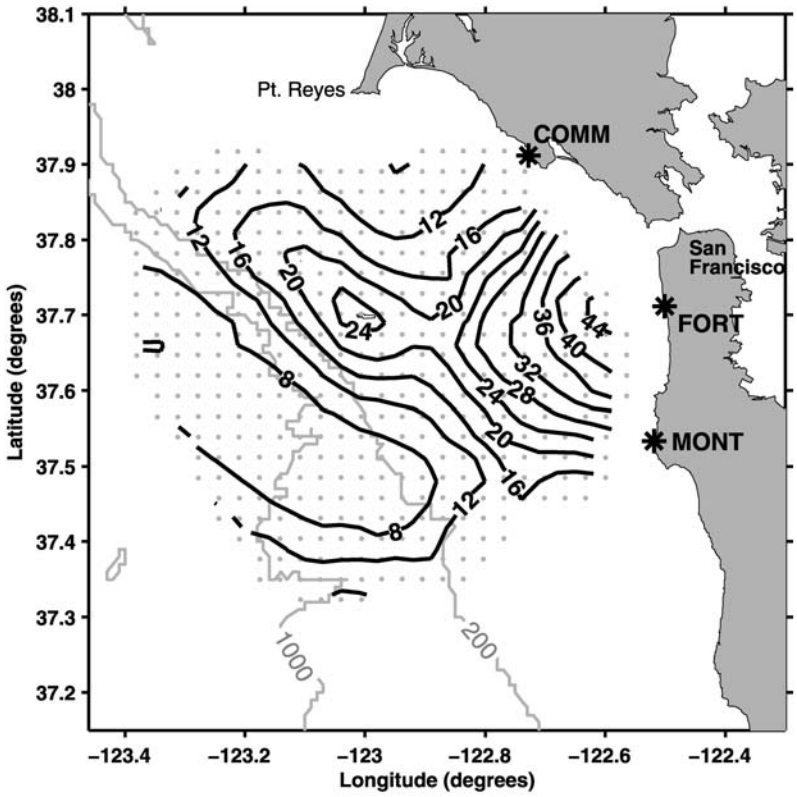

Figure 9. Percent total tidal variance contours for the year September–August 2006–2007. Grey dots indicate HF radar data points.

4.2. Harmonic Tidal Analyses on Buoy 46026 Winds

[42] The harmonic tidal analysis on a year of buoy 46026 wind data did not identify a significant contribution for any tidal constituents (Table 2). By comparison, harmonic analyses on the three 4 month time periods did identify the K_1 constituent as having significant major axis amplitudes and signal-to-noise ratios (Table 3). This shows that K_1 and P_1 results generated by harmonic tidal analyses on surface currents performed over long time periods such as a year are less likely to be influenced by diurnal winds than those performed over shorter time periods.

5. Spectral Analyses on Winds and HF Radar Measured Surface Currents

[43] The rotary spectral analysis on 1 year of buoy 46026 wind stress data shows significant energy at low frequencies (<0.4 cpd) and well-defined peaks at diurnal and semidiurnal frequencies (Figure 4c). The diurnal peak is almost certainly due to the influence of the diurnal sea breeze. The semidiurnal peak is most likely due to the generation of wind-forced energy in the first even harmonic of the predominant diurnal frequency [*Militello and Kraus*, 2001]. CW energy is slightly larger than CCW energy in the diurnal band and the semidiurnal CW peak is broader and shifted toward lower frequencies.

[44] The rotary spectral analysis on surface current vectors demonstrates a dominant CW-oriented energy peak at the diurnal frequency and a dominant CCW-oriented energy peak at the semidiurnal frequency (Figure 4a). This is reflected in the K_1 and M_2 tidal ellipse plots where the diurnal K_1 is CW throughout the gulf and the semidiurnal M_2 is CCW over the shelf (Figure 11). There is an indication of a CW peak at a slightly greater frequency than the diurnal frequency (Figure 4a) which is most likely due to inertial currents as the inertial frequency is 1.22 cpd in this region. This inertial peak is approximately half the amplitude of the diurnal peak, exhibited CW energy an order of magnitude greater than the CCW energy, and was a dominant peak in the residual spectral plot.

[45] Residual current spectra show the removal of both CW and CCW energy at the diurnal frequency and CCW energy at the semidiurnal frequency (Figure 4b) which is consistent with the removal of K_1 and M_2 tidal currents. A more complete removal of energy in the CW-oriented diurnal peak is most likely due to the influence of the CW dominance of diurnal wind stress and the periodic diurnal signal in the residual time series (Figure 3).

[46] For the most part, spectral analyses on surface currents analyzed on the 11 shorter time periods exhibited identifiable peaks at semidiurnal, diurnal, and inertial frequencies (Figures 5 and 6) although there are some notable variations. There appears to have been a decrease in diurnal CW (but not CCW) energy between January and April (not pictured). The harmonic tidal analysis also showed a decrease in tidal energy during this time.

[47] There are some vague trends that can be seen in the wind stress spectral analyses on the 11 time periods. Some months had definite diurnal and semidiurnal peaks but they did not seem correlated with the total amount of energy in

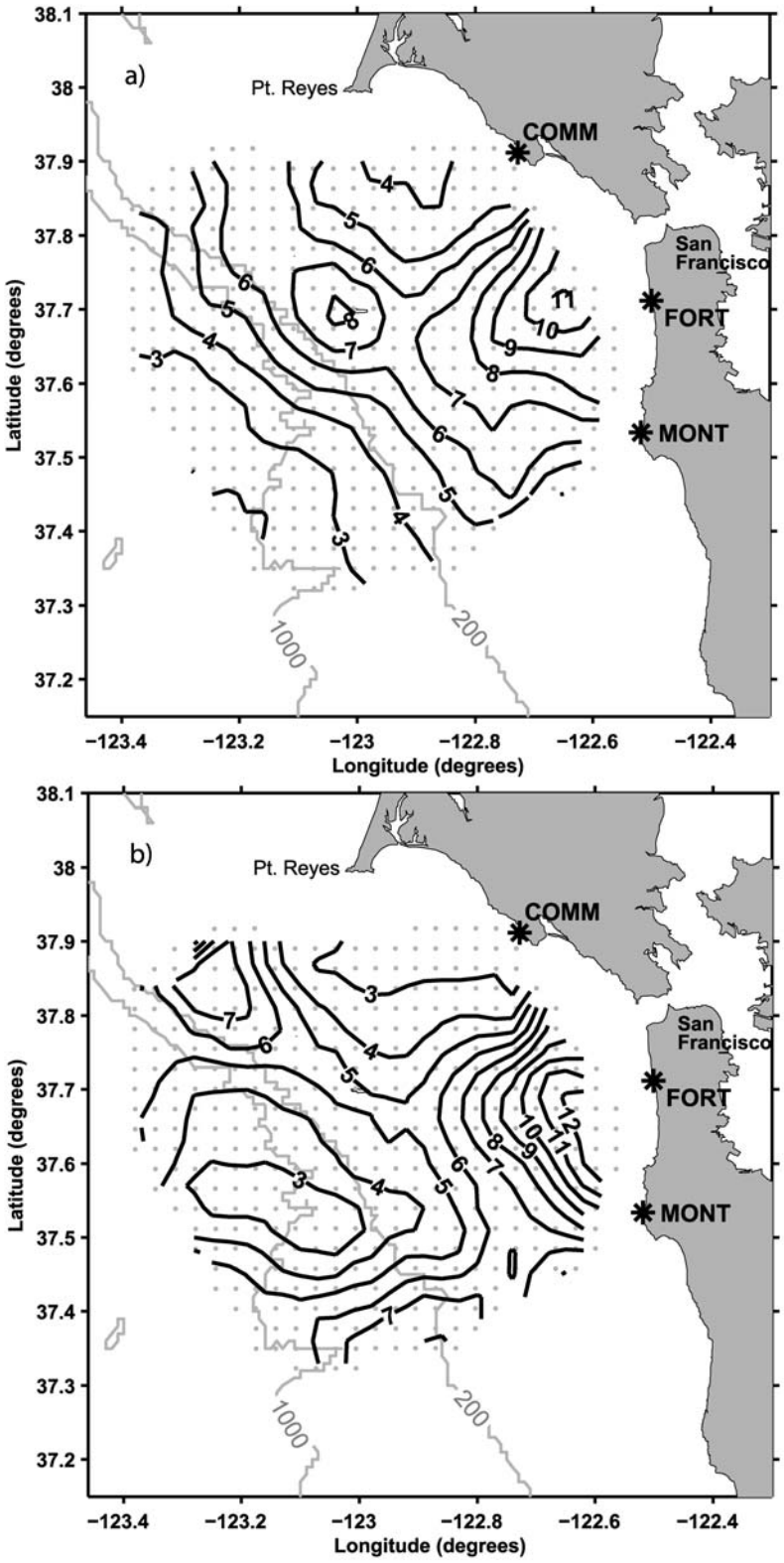

Figure 10. (a) K_1 and (b) M_2 tidal ellipse major axis amplitude contours in cm/s for the year September–August 2006–2007. Grey dots indicate HF radar data points.

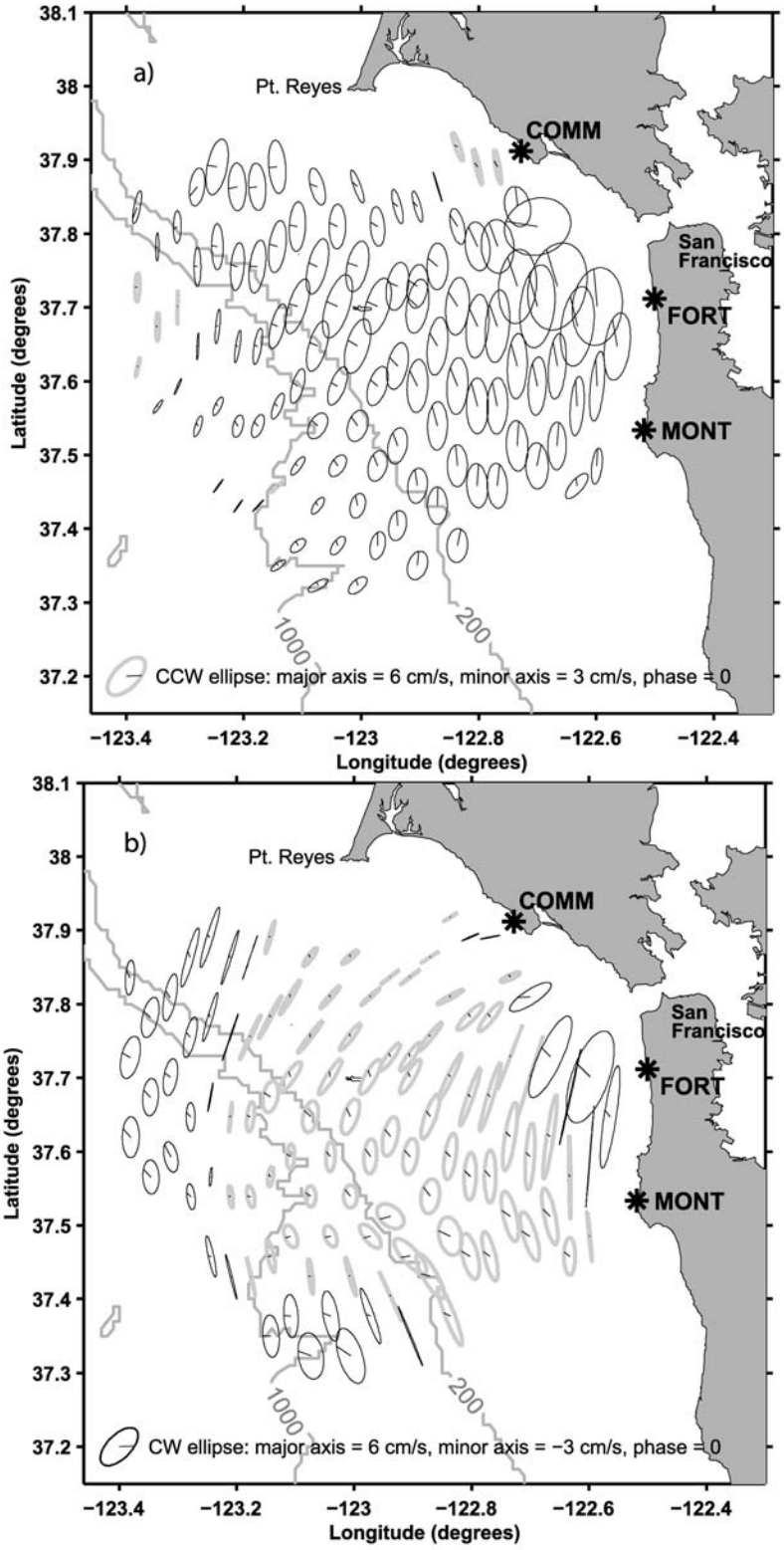

Figure 11. (a) K_1 and (b) M_2 tidal ellipses derived from the harmonic tidal analysis on a year of HF radar data (September–August 2006–2007). Ellipses are for every fourth HF radar data point. CCW ellipses are gray, CW ellipses are black, and black lines emanating from the center of ellipses denote phase relative to UT.

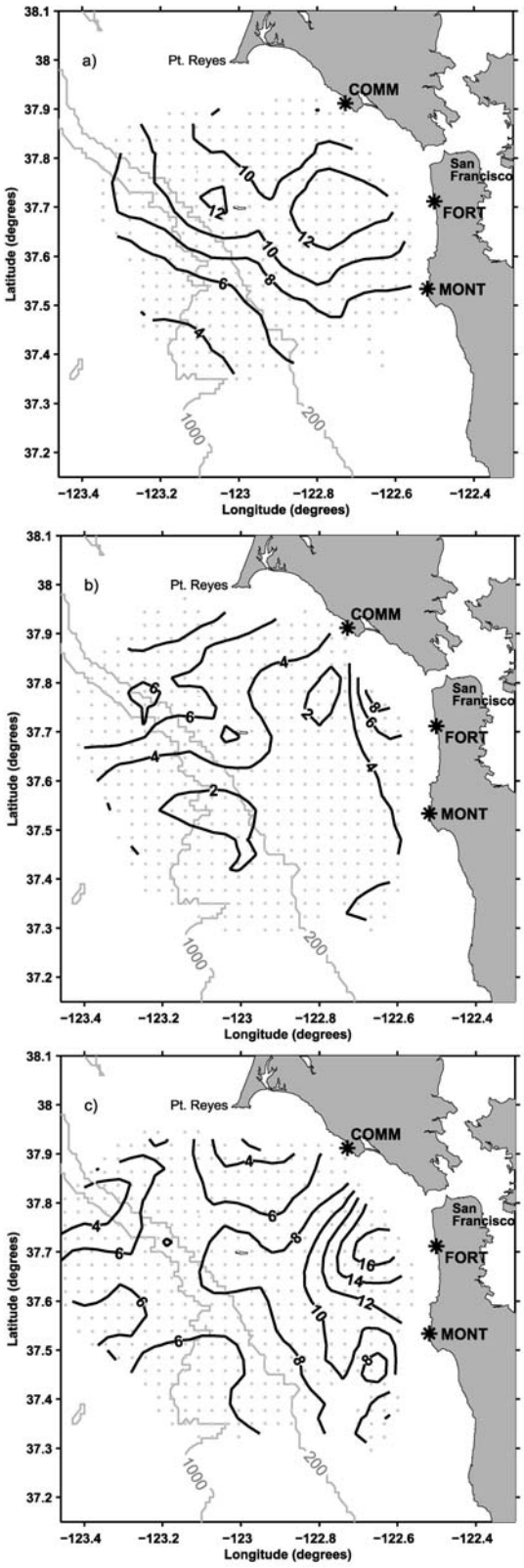

Figure 12. Contours of K_1 ellipse major axis amplitudes in cm/s derived from harmonic tidal analyses performed on HF radar data for three separate 4 month time periods: (a) September–December 2006, (b) January–April 2007, and (c) May–August 2007. Grey dots indicate HF radar data points.

the winds. For example, March and April did not exhibit definite diurnal signals despite having the most energetic winds (Figure 6). September, on the other hand, had characteristically light winds but had the most obvious diurnal peak (Figure 5). June, July, and August also exhibited definite diurnal signals despite having lower than average wind energy (not pictured). In general, it appears that the amplitudes of the diurnal and semidiurnal peaks remain fairly constant throughout the year. It is the energy in all other frequencies that change as these frequencies exhibited significantly more energy during the upwelling season compared to the relaxation season. This can be seen comparing Figures 5 (relaxation period PSD) and 6 (upwelling period PSD). In contrast, *Rosenfeld* [1988] found that periods of strong upwelling winds coincided with large diurnal wind stress along the Bodega Bay region to the north.

6. Discussion

6.1. Seasonal Surface Flow and Divergence Patterns

[48] In general, our findings regarding the relaxation/upwelling/storm seasonal regimes agree with previous studies on seasonal surface flow patterns along the coast of central and northern California [*Gan and Allen*, 2002; *Hickey and Pola*, 1983; *Largier et al.*, 1993]. Discrepancies with these studies in both onset timing and spatial structure of the seasonal regimes are most likely due to our more continuous data set, natural seasonal variations in the meteorology and the gulf's unique coastline and bathymetry. The defined seasonal pattern that we observed is in disagreement with previous studies within the gulf that observed no seasonal pattern [*Noble and Ramp*, 2000; *Steger et al.*, 2000]. However, *Steger et al.* [2000] did not have the temporal resolution that we used and *Noble and Ramp* [2000] concentrated on subsurface flow beyond the shelf.

[49] For the relaxation period, October–December 2006, mean winds at buoy 46026 decreased from mean winds during the spring and summer months. Mean surface flow patterns responded by developing strong poleward flow over the slope. It is fairly well documented that poleward flow during the relaxation period is due to a large-scale alongshore sea surface pressure gradient [*Gan and Allen*, 2002; *Hickey and Pola*, 1983; *Largier et al.*, 1993]. Even though there was significant poleward flow over the slope, flow over most of the shelf, particularly in the southern regions, remained equatorward (with the exception of December; Figure 7). This equatorward flow is not believed to be driven by a cross-shelf barotropic pressure gradient set up by offshore Ekman transport since winds typically are not persistent or strong enough to develop significant Ekman transport. However, the equatorward flow over the shelf does appear to be linked to the winds. Of the 3 months during relaxation, October exhibited the strongest mean winds from the northwest and the strongest equatorward flow over the shelf while December exhibited very weak mean winds and no defined equatorward flow over the shelf. Wind stress could therefore be directly driving the equatorward flow over the shelf during relaxation and only diminishing the pressure gradient driven poleward flow over the slope.

[50] The gulf has been observed to be an important retention region of San Francisco Bay outflow, oceanic, and

newly upwelled water [*Wing et al.*, 1998]. Mean monthly flow patterns during the relaxation and storm periods hint at the following two eddy patterns south of Pt. Reyes potentially associated with retentive circulation: (1) a cyclonic eddy pattern appears to develop off the poleward flow following the coast north of the Bay's mouth and southward flow south of the tip of Pt. Reyes (Figures 7 and 8) and (2) to the west, an anticyclonic eddy pattern appears to develop within the region of shear between the poleward relaxation flow over the slope and equatorward flow south of the tip of Pt. Reyes in December (Figure 7). July and August also exhibit a weak eddy pattern west of the mouth of the Bay (Figure 8). Further investigation into these eddy patterns by examining hourly surface flow patterns could illuminate their longevity, strength, and significance.

[51] We examined two 24 hour periods of hourly surface flow patterns during the relaxation period: 2 October 2006 1700 UT to 3 October 2006 1600 UT and 3 November 2006 0400 UT to 4 November 2006 0300 UT (not pictured). These two periods were chosen based on low winds recorded at buoy 46026 so that wind-driven flow could be dismissed. Although a well-defined eddy pattern like the one mentioned above (south of Pt. Reyes) was not observed during these two time periods, an eddy can briefly be seen between 3 October 2006 0100 and 0400 UT. This eddy was most likely enhanced by wind stress-driven flow off Point Reyes (it is not uncommon for winds off Point Reyes to be greater than those observed at buoy 46026). Between 3 November 2006 2200 UT and 4 November 2006 0400 UT an anticyclonic eddy developed in the shear environment between the equatorward flow over the shelf and poleward flow over the slope. *Steger et al.* [2000] observed a similar anticyclonic eddy form in the same region.

[52] The poleward flow observed over the slope during the relaxation season could be the surfacing of the California Undercurrent. *Noble and Ramp* [2000] observed the California Undercurrent in this region where the continental shelf widens to be surface intensified, cross isobaths and veer offshore. *Steger et al.* [2000] found near-surface water over the slope to contain high temperatures and salinities associated with Pacific Equatorial Water. AVHRR satellite images of sea surface temperatures for 11 and 14 November 2007 showed a tongue of warm sea surface temperatures (15–16°C) over the slope entering the Gulf of the Farallones from the south [*Gough*, 2008] but, without CTD measurements it is difficult to determine the origin of these waters. Poleward flow over the slope continued to influence the mean circulation during the storm season. This can be seen in the westward deflection of the flow over the slope in January and February (Figure 7).

[53] The storm season surface flow is strongly influenced by highly variable storm-driven wind stress. The identification of generalized flow characteristics from mean monthly patterns are therefore difficult to make. Although the mean winds at buoy 46026 had small magnitudes for December and February (Figure 7), wind stress during these months displayed some of the highest values during the year in both the northward and southward directions (Figure 3). These dramatic switches in wind stress are typical of powerful northward winds associated with atmospheric cyclonically rotating low-pressure systems approaching from the west and southward winds associated with low-pressure systems departing to the east. January did not exhibit these switches in wind stress direction (Figure 3). Winds during January exhibited periods of strong winds from the north and periods of winds from the east. We speculate that the region of strong southwestward flow apparently emanating from the mouth of the Bay could have been influenced by strong offshore wind events funneled through the gap in the coastal range. Buoy 46026 winds did not exhibit strong westward winds since the buoy is located outside of this region, but residual currents in this region showed strong peaks in westward flow between 4 and 10 January [*Gough*, 2008]. These peaks strongly influenced the mean flow in January since there was a 6 day data gap and there were light winds at the end of the month.

[54] There is evidence of poleward flow out of the San Francisco Bay behaving like a coastally trapped low-salinity buoyancy flow that follows the coast to the north [*Wiseman and Garvine*, 1995] during the relaxation and storm season. Although we cannot observe the flow in/out of the Bay with these data, we do have data within 20 km of the mouth of the Bay. The flow from the Bay tends to diverge with most flow veering equatorward (as mentioned above) and a narrow band of flow veering poleward. The strength and size of this poleward flow in the mean monthly flow patterns appear to be correlated with monthly precipitation totals. November, December, and February saw the most rainfall and demonstrated the strongest evidence of coastally trapped buoyancy flow patterns (Figure 7). Monthly precipitation totals of 7.7, 13.5, and 12.2 cm were recorded at downtown San Francisco for the months of November, December, and February (www.ggweather.com). Buoyancy flow patterns can be seen to a lesser extent in September and October (Figure 7). Evidence of coastally trapped buoyancy flow out of the San Francisco Bay can also be seen in hourly surface flowcharts (not pictured) following heavy precipitation events.

[55] There was a sudden striking change in the wind regime in March which marked the beginning of the upwelling season. Surface flow patterns immediately responded to strong winds from the northwest and became equatorward throughout the region. The spatial pattern of the flow, particularly over the slope and away from the strong tidal influence near the mouth of the Bay, most likely reflects patterns in the wind field. Where flow enters the gulf from the north, mean surface flow split in the following two directions during the months of March, April, and May (Figure 8): (1) the western split flows southward over the slope and is very strong and (2) the eastern split is significantly weaker and veers toward the east. The longitudinal location of the split varied between the 3 months. The eastern split in the flow is not believed to be significantly influenced by tidal currents as the tidal variance in this region is small. Therefore, at this time, we believe that the weak flow in the eastern split is a reflection of subtidal influences (weak wind stress and periodic poleward flow). *Wing et al.* [1998] described periodic poleward flow south of Point Reyes during the upwelling season and *Wright* [2008] observed poleward flow in this region in April 2008. Further investigation of hourly flow patterns in this region could illuminate the timing, duration, and strength of this periodic poleward flow. Examination of hourly flow patterns during strong persistent winds in the upwelling

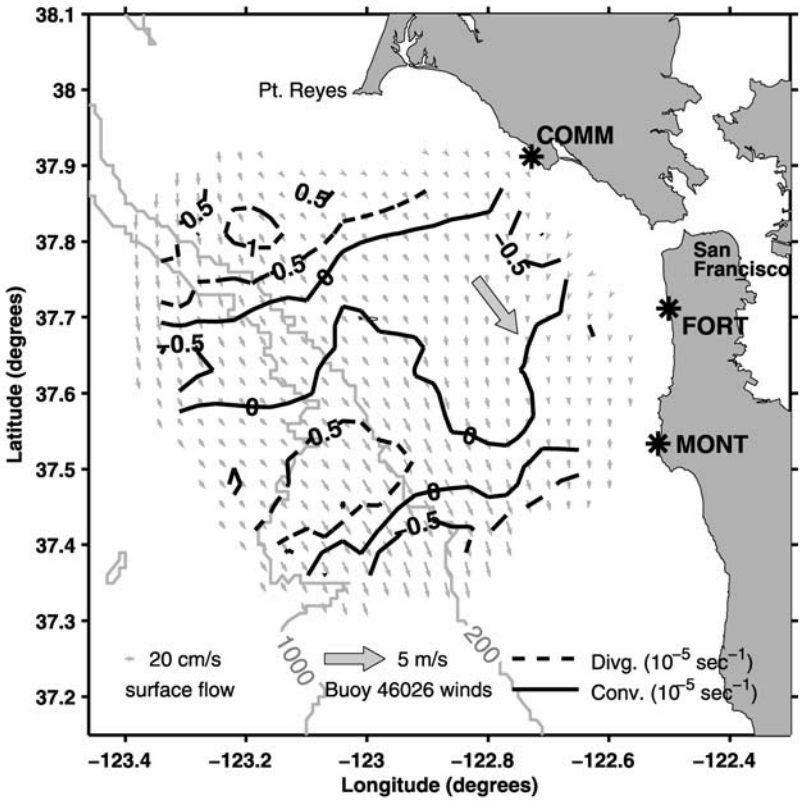

Figure 13. Mean divergence contours averaged over the beginning of the upwelling season of 2007 (March, April, and May). Dashed contours indicate divergence and solid contours indicate negative divergence (convergence) on the order of 10^{-5} s^{-1}. Small gray arrows indicate mean surface flow scaled down to primarily show direction. The large gray arrow indicates magnitude and direction of mean winds at buoy 46026.

season (not pictured) did not reveal poleward flow south of Point Reyes although it would be expected that this poleward flow would typically manifest itself during periods of diminished upwelling-favorable winds.

[56] During the upwelling months, there is a semicircular region of weakened mean surface currents that extends about 50 km out from the Fort Funston HF radar station (Figure 8). This region of weakened currents, which reflects the shape of the tidal variance field (Figure 9), is likely due to a combination of decreased wind stress and increased tidal influence.

[57] There was a persistent structure to the mean monthly divergence patterns that began in March, was accentuated in April and May, and remained (to a lesser degree) until June (Figure 13). This included areas of divergence southwest of Pt. Reyes and in the southwest region of the study area. These two regions of divergence were separated by a region of convergence. The region of divergence to the southwest is not a well-documented region of upwelling like Bodega Bay to the north and Año Nuevo to the south, but it could be important, from a biological standpoint, considering the flow out of the bay is typically directed equatorward toward this region of possible upwelling. No persistent structure to divergence was observed during the relaxation season.

[58] *Steger et al.* [2000] noted that AVHRR satellite images of sea surface temperatures typically show a region of cool temperatures just south of Pt. Reyes. It is widely believed that cool waters south of Pt. Reyes are advected from Bodega Bay upwelling regions to the north [*Kaplan and Largier*, 2006; *Steger et al.*, 2000; *Wing et al.*, 1998]. This appears to be true, but mean monthly divergence patterns during the upwelling season of 2007 show a region of persistent divergence southwest of Pt. Reyes. This divergent pattern was strongest in April [*Gough*, 2008] and appears to have been enhanced by the split in the flow observed off Pt. Reyes (Figure 8). This persistent divergence pattern implies that cool sea surface temperatures during upwelling events could be due to local upwelling in addition to cold water advection from the north.

6.2. Tidal Currents and the Effects of Diurnal Winds on Harmonic Tidal Analyses

[59] The tidal currents in the Gulf of the Farallones are highly variable due to the complex bathymetry and strong tidal influence from flow entering and exiting the San Francisco Bay. Adding to the complexity of the surface currents is the temporal and spatial variability of the wind's influence. Strong nontidal surface flow driven by diurnal wind stress is of particular concern since it can mimic diurnal tidal currents and corrupt harmonic tidal analyses. Our results show that harmonic tidal analyses performed over longer time frames, such as a year, are more effective at disassociating diurnal wind-driven currents from diurnal tidal currents than those performed over seasonal time frames.

Table 4. Summary of Subtidal Correlations With Winds and Total Tidal Variance Percentages at Four Cross-Shore Locations

Point	U Winds Versus V Residuals (R^2)	V Winds Versus V Residuals (R^2)	Total Tidal Variance (%)
A	0.25	0.56	32.8
B	0.28	0.46	14.9
C	0.28	0.41	8.9
D	0.14	0.24	5.2

[60] The rotational orientation of K_1 tidal ellipses were essentially clockwise (CW) throughout the gulf and not necessarily aligned with the continental margin. This is consistent with the category 2 barotropic diurnal tide behaving as a combination of Kelvin and continental shelf waves [*Noble et al.*, 1987]. The rotational orientation of the K_1 also agreed with observations by *Kaplan et al.* [2005] off Bodega Bay where the K_1 ellipses rotated CW throughout the region. A switch from poleward flow to equatorward flow during periods of low winds and spring tides (2 October 2006 1700 UT to 3 October 2006 1600 UT and 3 November 2006 0400 UT to 4 November 2006 0300 UT, not pictured) was observed to begin after high tide as a narrow band of equatorward flow near the coast that gradually spread across the shelf as the tide receded. This is supported by nearshore K_1 tidal ellipse phases leading the farshore phases in Figure 11.

[61] Previous studies have shown that the M_2 ellipses are highly variable in both magnitude and rotational direction off Bodega Bay [*Kaplan et al.*, 2005; *Noble et al.*, 1987]. *Noble et al.* [1987] attributes these perturbations in the M_2 as characteristics of coastally trapped Kelvin waves affected by variations in the coastal boundary. Our results also show that M_2 ellipses had noticeably varied amplitudes, eccentricity, inclination, and rotational orientation (Figure 11b). There is an indication that the rotational direction of M_2 ellipses switch direction at the outer shelf (CCW over the shelf and CW over the slope) although this switch is not as well defined as what *Kaplan et al.* [2005] found in the Bodega Bay region. *Kaplan et al.* [2005] believed the switch in the M_2 ellipse rotation to be indicative of internal tidal waves propagating both toward and away from the shelf break.

[62] Our findings validate observations by *Steger et al.* [1998] that there is an area near 37.5°N, 123.0°W where tidal velocities are very small. HF radar data has allowed us to see the size of this region which extends along the slope and is where the K_1 and M_2 amplitudes have diminished (Figure 10) along with the tidal variance (Figure 9). In this region the P_1, O_1, S_2 and K_2 have comparable amplitudes to the K_1 and M_2 (Table 1) which were in the 1–3 cm/s range. HF radar has also allowed us to identify another region south of Pt. Reyes where tidal variances are small (Figure 9).

[63] Effective discernment of K_1 tidal currents from diurnal wind-driven currents in the yearlong data set is supported by the following evidence: (1) Harmonic tidal analysis on buoy 46026 wind data showed relatively small amplitudes and signal-to-noise ratios for the K_1 frequency (Table 2), (2) there is a significant phase difference between the K_1 surface currents (Table 1) and K_1 winds (Table 2) in their respective harmonic analyses, and (3) the removal of most of the diurnal oscillation in the residual current time series (Figure 3). The intermittent diurnal oscillation in the residuals often occurs when the diurnal wind stress is in phase with the diurnal tidal currents, but it also occurs occasionally when there is no evidence of diurnal wind stress (Figure 3). This could be due to currents affected by nearshore diurnal sea breezes shoreward of (and therefore not measured by) buoy 46026 and the varying spatial extent of tidal currents influenced by the spring/neap cycle causing widely variable tidal current amplitudes not determined in harmonic analysis.

[64] Evidence that harmonic tidal analyses performed over seasonal time frames (4 months in this case) did not discern K_1 tidal currents from diurnal wind-driven currents as well as yearlong analyses is supported by the following: (1) the harmonic tidal analyses on buoy 46026 wind data using the 4 month data sets showed significant K_1 amplitudes and signal-to-noise ratios (Table 3) and therefore could infiltrate harmonic analyses on currents and (2) widely variable K_1 major axis amplitudes in the 4 month time periods in the harmonic analyses on surface currents (Figure 12).

6.3. Correlations Between Wind-Driven and Residual Currents

[65] Tidal currents and wind-driven currents make up a greater percentage of the surface currents at nearshore locations compared to far-shore locations. This is exhibited by the high nearshore total tidal variance values and strong nearshore winds versus residuals correlations (Table 4). Thus, we have a better statistical understanding of currents closer to shore.

[66] Poor correlations between buoy 46026 winds and residual currents during the upwelling season are most likely due to the winds over the slope differing from those measured at the buoy. Assuming the surface flow patterns during the upwelling season are largely reflective of the winds, it is reasonable to believe that the wind patterns are also quite variable over the gulf as equatorward surface flow over the slope is noticeably greater than that found near the buoy and inner shelf (Figure 8). *Dorman and Winant* [1995] observed a significant decrease in winds at buoy 46026 compared to winds recorded at buoys to the north and south. Poor correlations at far-shore locations during the relaxation season are most likely due to poleward surface flow over the slope while light winds continue to blow from the northwest. Perhaps there is more of a time lag response in the currents when there is a "relaxing" of the winds. Previous studies have shown a surface current time lag response to winds [*Kaplan et al.*, 2005; *Noble et al.*, 1992]. Poor correlations could also be influenced by a veering of surface currents due to Ekman transport, inertial effects, wind stress curl, eddies or flow from the Bay.

7. Summary

[67] The high spatial and temporal resolution surface flow patterns measured with HF radar has illuminated some of the intricacies in the flow in addition to confirming some of the general relaxation/storm/upwelling seasonal trends found in previous studies conducted along central and northern California.

[68] There was strong poleward flow over the continental slope during the relaxation months (October–December

2006). Although flow was typically poleward over the slope during relaxation, mean flow over the shelf was typically equatorward (except December 2006). Poleward flow over the slope and equatorward flow over the shelf tend to meet along the outer shelf, this pattern is most strongly evident during November 2006 where there was an abrupt change in flow direction along the 200 m isobath.

[69] Equatorward flow dominated throughout the region during the upwelling months (March–June 2007). Strong equatorward flow was found off Point Reyes with weaker flow south and inshore of Point Reyes veering toward the east. The longitudinal location of the split in this flow varied from month to month and is most likely a reflection of the wind field. This is also the region that exhibited the strongest mean divergence patterns. Mean divergence patterns show a persistent divergence structure during the upwelling season with divergence at the northern and southern regions of the gulf separated by a region of convergence.

[70] Mean monthly flow patterns during months of heavy precipitation provide evidence of a coastally trapped buoyancy flow out of the mouth of the Bay. From this flow, it appears that a cyclonic eddy can develop. West of this cyclonic eddy, an anticyclonic eddy can develop from the equatorward flow south of the tip of Pt. Reyes and poleward flow over the slope during relaxation. These eddy patterns appear to define the Gulf of the Farallones retention areas.

[71] Harmonic tidal analyses performed on surface currents over longer time frames such as a year appear to be more effective at disassociating diurnal wind-driven currents from diurnal tidal currents compared to harmonic tidal analyses over seasonal time frames. This is most likely due to seasonal shifts in the timing of the diurnal sea breeze that are not identified at the fixed K_1 harmonic in the yearlong analysis.

[72] K_1 tidal ellipses were found to be roughly correlated with the bathymetry as major axis amplitudes increased and were oriented alongshore over much of the shelf (with the exception of near the mouth of the San Francisco Bay). This is consistent with category 2 barotropic diurnal tides behaving as a combination of Kelvin and continental shelf waves. M_2 tidal ellipses were variable in amplitude, eccentricity, inclination and rotational orientation which are consistent with the M_2 tide behaving as a coastally trapped Kelvin wave. The indication of a switch in the directional orientation of M_2 ellipses near the shelf break are attributed to internal tide propagation both toward and away from the shelf break. The percentage of original HF radar surface currents due to tidal influences (i.e., the tidal variance) reflects the combined contribution of the K_1 and M_2 constituents. Although the K_1 and M_2 dominated the tidal flow in the gulf, the P_1 and O_1 amplitudes were comparable in magnitude over the slope.

[73] Nearshore regions, when compared to farshore regions, had higher tidal variance and showed stronger correlations between winds and residual currents. Therefore, a significantly larger percentage of nearshore currents in the Gulf of the Farallones can be explained by wind and tidal forcing as opposed to the offshore regions that are dominated by large-scale oceanic circulation.

[74] **Acknowledgments.** This project was funded by the California Ocean Current Monitoring Program (COCMP). Two anonymous reviewers provided excellent suggestions and comments that greatly improved the paper. We would like to thank Jim Pettigrew and Dwight Peterson from RTC for their help with data collection and MATLAB programming. Regan Long (CODAR), along with the rest of the CODAR team, provided crucial technical support and assistance with HF radar data processing. David Kaplan (UC Santa Cruz) provided the tidal ellipse MATLAB program among other assistance and Fred Bahr (Naval Post Graduate School) provided the rotary spectral MATLAB program. Leonard Sklar (San Francisco State University) and Jeff Paduan (Naval Postgraduate School) provided counsel on statistical and error analyses.

References

Barrick, D. E., and B. J. Lipa (1979), A compact transportable HF radar system for directional coastal wave field measurements, in *Ocean Wave Climate*, edited by M. D. Earle and A. Malahoff, pp. 153–201, Plenum, New York.

Beardsley, R. C., and S. J. Lentz (1987), The Coastal Ocean Dynamics Experiment collection: An introduction, *J. Geophys. Res.*, *92*(C2), 1455–1463, doi:10.1029/JC092iC02p01455.

Beardsley, R. C., R. Limeburner, and L. K. Rosenfeld (1985), CODE 2: Moored array and large-scale data report, data report, 31 pp., Woods Hole Oceanogr. Inst., Woods Hole, Mass.

Brink, K. H., and T. J. Cowles (1991), The coastal transition zone program, *J. Geophys. Res.*, *96*(C8), 14,637–14,647, doi:10.1029/91JC01206.

Carbajal, N., and T. Pohlmann (2004), Comparison between measured and calculated tidal ellipses in the German Bight, *Ocean Dyn.*, *54*, 520–530, doi:10.1007/s10236-004-0096-5.

Chapman, R. D., L. K. Shay, H. C. Graber, J. B. Edson, A. Karachintsev, C. L. Trump, and D. B. Ross (1997), On the accuracy of HF radar surface current measurements: Intercomparisons with ship-based sensors, *J. Geophys. Res.*, *102*(C8), 18,737–18,748, doi:10.1029/97JC00049.

Dorman, C. E., and C. D. Winant (1995), Buoy observations of the atmosphere along the west coast of the United States, 1981–1990, *J. Geophys. Res.*, *100*(C8), 16,029–16,044, doi:10.1029/95JC00964.

Dorman, C. E., T. Holt, D. P. Rogers, and K. Edwards (2000), Large-scale structure of the June–July 1996 marine boundary layer along California and Oregon, *Mon. Weather Rev.*, *128*, 1632–1652, doi:10.1175/1520-0493(2000)128<1632:LSSOTJ>2.0.CO;2.

Gan, J., and J. S. Allen (2002), A modeling study of shelf circulation off northern California in the region of the Coastal Ocean Dynamics Experiment: 2. Simulations and comparisons with observations, *J. Geophys. Res.*, *107*(C11), 3184, doi:10.1029/2001JC001190.

Gonella, J. (1972), Rotary-component method for analyzing meteorological and oceanographic vector time series, *Deep Sea Res.*, *19*(12), 833–846.

Gough, M. (2008), An analysis of HF-radar measured surface currents, Gulf of the Farallones, California, M.Sc. thesis, San Francisco State Univ., San Francisco, Calif.

Hickey, B. M., and N. E. Pola (1983), The seasonal alongshore pressure gradient on the west coast of the United States, *J. Geophys. Res.*, *88*(C12), 7623–7633, doi:10.1029/JC088iC12p07623.

Huyer, A., J. A. Barth, P. M. Kosro, R. K. Shearman, and R. L. Smith (1998), Upper-ocean water mass characteristics of the California current, summer 1993, *Deep Sea Res. Part II*, *45*(8–9), 1411–1442, doi:10.1016/S0967-0645(98)80002-7.

Kaplan, D. M., and J. Largier (2006), HF radar-derived origin and destination of surface waters off Bodega Bay, California, *Deep Sea Res. Part II*, *53*(25–26), 2906–2930, doi:10.1016/j.dsr2.2006.07.012.

Kaplan, D. M., J. Largier, and L. W. Botsford (2005), HF radar observations of surface circulation off Bodega Bay (northern California, USA), *J. Geophys. Res.*, *110*, C10020, doi:10.1029/2005JC002959.

Kohut, J. T., and S. M. Glenn (2003), Improving HF radar surface current measurements with measured antenna beam patterns, *J. Atmos. Oceanic Technol.*, *20*(9), 1303–1316, doi:10.1175/1520-0426(2003)020<1303:IHRSCM>2.0.CO;2.

Large, W. G., and S. Pond (1981), Open ocean momentum flux measurements in moderate to strong winds, *J. Phys. Oceanogr.*, *11*(3), 324–336, doi:10.1175/1520-0485(1981)011<0324:OOMFMI>2.0.CO;2.

Largier, J. L., B. A. Magnell, and C. D. Winant (1993), Subtidal circulation over the northern California shelf, *J. Geophys. Res.*, *98*(C10), 18,147–18,179, doi:10.1029/93JC01074.

Largier, J. L., et al. (2006), WEST: A northern California study of the role of wind-driven transport in the productivity of coastal plankton communities, *Deep Sea Res. Part II*, *53*(25–26), 2833–2849, doi:10.1016/j.dsr2.2006.08.018.

Lipa, B., B. Nyden, D. S. Ullman, and E. Terrill (2006), SeaSonde radial velocities: Derivation and internal consistency, *IEEE J. Oceanic Eng.*, *31*(4), 850–861.

Long, R. M. (2007), Surface current measurements during safe seas 2006: Comparison and validation of measurements from high-frequency radar and the quick release environmental buoy, paper presented at Oceans 2007 Conference, Mar. Technol. Soc., Inst. of Electr. and Electr. Eng., Vancouver, B. C., Canada.

Lynn, R. J., and J. J. Simpson (1987), The California Current System: The seasonal variability of its physical characteristics, *J. Geophys. Res.*, *92*(C12), 12,947–12,966.

Militello, A., and N. C. Kraus (2001), Generation of harmonics by sea breeze in nontidal water bodies, *J. Phys. Oceanogr.*, *31*(6), 1639–1647, doi:10.1175/1520-0485(2001)031<1639:GOHBSB>2.0.CO;2.

Noble, M., L. K. Rosenfeld, R. L. Smith, J. V. Gardner, and R. C. Beardsley (1987), Tidal currents seaward of the northern California continental shelf, *J. Geophys. Res.*, *92*(C2), 1733–1744, doi:10.1029/JC092iC02p01733.

Noble, M., S. R. Ramp, and K. Kinoshita (1992), Current patterns over the shelf and slope adjacent to the Gulf of the Farallones: Executive summary, *U.S. Geol. Surv. Open File Rep., 92-382*, 1–26.

Noble, M. A., and S. R. Ramp (2000), Subtidal currents over the central California slope: Evidence for offshore veering of the undercurrent and for direct, wind-driven slope currents, *Deep Sea Res. Part II*, *47*(5–6), 871–906, doi:10.1016/S0967-0645(99)00130-7.

Ohlmann, C., P. White, L. Washburn, E. Terrill, B. Emery, and M. Otero (2007), Interpretation of coastal HF radar-derived surface currents with high-resolution drifter data, *J. Atmos. Oceanic Technol.*, *24*(4), 666–680, doi:10.1175/JTECH1998.1.

Paduan, J. D., and L. K. Rosenfeld (1996), Remotely sensed surface currents in Monterey Bay from shore-based radar (Coastal Ocean Dynamics Applications Radar), *J. Geophys. Res.*, *101*(C9), 20,699–20,686.

Paduan, J. D., K. C. Kim, M. S. Cook, and F. P. Chavez (2006), Calibration and validation of direction-finding high-frequency radar ocean surface current observations, *IEEE J. Oceanic Eng.*, *31*(4), 862–875, doi:10.1109/JOE.2006.886195.

Pawlowicz, R., B. Beardsley, and S. Lentz (2002), Classical tidal harmonic analysis including error estimates in MATLAB using T_TIDE, *Comput. Geosci.*, *28*(8), 929–937, doi:10.1016/S0098-3004(02)00013-4.

Rosenfeld, L. K. (1988), Diurnal period wind stress and current fluctuations over the continental-shelf off northern California, *J. Geophys. Res.*, *93*(C3), 2257–2276, doi:10.1029/JC093iC03p02257.

Steger, J. M., C. A. Collins, F. B. Schwing, M. Noble, N. Garfield, and M. T. Steiner (1998), An empirical model of the tidal currents in the Gulf of the Farallones, *Deep Sea Res. Part II*, *45*(8–9), 1471–1505, doi:10.1016/S0967-0645(98)80004-0.

Steger, J. M., F. B. Schwing, C. A. Collins, L. K. Rosenfeld, N. Garfield, and E. Gezgin (2000), The circulation and water masses in the Gulf of the Farallones, *Deep Sea Res. Part II*, *47*, 907–946, doi:10.1016/S0967-0645(99)00131-9.

Ullman, D., J. O'Donnell, C. Edwards, T. Fake, D. Morschauser, M. Sprague, A. Allen, and L. B. Krenzien (2003), Use of Coastal Ocean Dynamics Radar (CODAR) technology in U.S. Coast Guard search and rescue planning, final report, Res. and Dev. Cent., U.S. Coast Guard, Washington, D. C.

Wing, S. R., L. W. Botsford, S. V. Ralston, and J. L. Largier (1998), Meroplanktonic distribution and circulation in a coastal retention zone of the northern California upwelling system, *Limnol. Oceanogr.*, *43*, 1710–1721.

Wiseman, W., and R. Garvine (1995), Plumes and coastal currents near large river mouths, *Estuaries Coasts*, *18*(3), 509–517, doi:10.2307/1352368.

Wright, G. (2008), Validation of high frequency radar used in ocean surface current mapping via in-situ drifting buoys, M.Sc. thesis, Nav. Postgrad. Sch., Monterey, Calif.

N. Garfield and M. K. Gough, Romberg Tiburon Center for Environmental Studies, San Francisco State University, 3152 Paradise Dr., Tiburon, CA 94920, USA. (interbag@hotmail.com)

E. McPhee-Shaw, Moss Landing Marine Laboratories, San Jose State University, 8272 Moss Landing Rd., Moss Landing, CA 95039, USA.